Journal of Nuclear Materials 405 (2010) 207–215

Contents lists available at ScienceDirect

Journal of Nuclear Materials

journal homepage: www.elsevier.com/locate/jnucmat

Air oxidation of Zircaloy-4 in the 600–1000 °C temperature range: Modeling for ASTEC code application

O. Coindreau [a,*], C. Duriez [a], S. Ederli [b]

[a] Institut de Radioprotection et de Sûreté Nucléaire, Major Accident Prevention Division, Cadarache Nuclear Center, France
[b] Italian National Agency for New Technologies, Energy and Sustainable Economic Development, Roma, Italy

ARTICLE INFO

Article history:
Received 29 March 2010
Accepted 24 July 2010

ABSTRACT

Progress in the treatment of air oxidation of zirconium in severe accident (SA) codes are required for a reliable analysis of severe accidents involving air ingress. Air oxidation of zirconium can actually lead to accelerated core degradation and increased fission product release, especially for the highly-radiotoxic ruthenium. This paper presents a model to simulate air oxidation kinetics of Zircaloy-4 in the 600–1000 °C temperature range. It is based on available experimental data, including separate-effect experiments performed at IRSN and at Forschungszentrum Karlsruhe. The kinetic transition, named "breakaway", from a diffusion-controlled regime to an accelerated oxidation is taken into account in the modeling via a critical mass gain parameter. The progressive propagation of the locally initiated breakaway is modeled by a linear increase in oxidation rate with time. Finally, when breakaway propagation is completed, the oxidation rate stabilizes and the kinetics is modeled by a linear law. This new modeling is integrated in the severe accident code ASTEC, jointly developed by IRSN and GRS. Model predictions and experimental data from thermogravimetric results show good agreement for different air flow rates and for slow temperature transient conditions.

1. Introduction

During a low probability severe reactor accident, which may happen in a nuclear power plant in case of loss of fuel cooling along with the failure of safety systems, the reactor core, inadequately cooled, would be progressively damaged. Core dry-out is primarily driven by decay heat, until Zircaloy oxidation comes into play above 1500 K, increasing rod temperature significantly. Most investigations of core degradation during severe accidents have considered oxidation by steam but it was demonstrated that metallic core components can be exposed to more complicated gas mixtures, such as air. Core degradation in air might occur during reactor operation, in case of a core meltdown accident with subsequent reactor pressure vessel breaching, under shutdown conditions with the upper head of the vessel removed [1], in spent fuel storage pools after accidental loss of cooling [2] or in case of storage and transportation cask accidents [3].

Concerning impacts on safety, the presence of air can lead to accelerated oxidation of the Zircaloy cladding compared to that in steam, owing to the faster kinetics, while the 85% higher heat of reaction drives this process further. Air ingress is typically associated with poor heat transfer; the combined effect of these factors can give rise to an increased rate of assemblies degradation. Furthermore, the exposure of UO_2 to air at elevated temperatures can lead to increased release of some fission products, notably the highly-radiotoxic ruthenium [4,5] while the effect of air is likely to further weaken the oxidized cladding as a barrier against fission product release. These considerations have taken IRSN to launch a research program consisting of experimental investigations and development of an accurate modeling of air oxidation in the ASTEC safety code. The temperature domain of concern starts at about 600 °C, where the oxidation rate becomes significant enough to play a role on further temperature elevation of the fuel assemblies in air ingress scenarios.

The complexity of air oxidation of Zircaloy arises out of the simultaneous oxidation and nitriding processes. For a better understanding of the oxidation-nitriding mechanism, one should consider that it consists, at least, of the three following processes: (a) an external interface reaction step between the atmosphere and the zirconium cladding, (b) the diffusion of oxygen and/or nitrogen through the already formed oxynitride layer to the underneath metal–oxynitride interface, (c) an internal interface reaction step.

Before giving an overview of these mechanisms and their kinetics in the next paragraph, it is worthwhile making a point about the energetics of zirconium dioxide (ZrO_2) and zirconium nitride (ZrN) formation, which can be described by the following equations:

$$Zr + O_2 \rightarrow ZrO_2 \quad (1)$$

$$Zr + 0.5N_2 \rightarrow ZrN \quad (2)$$

* Corresponding author. Tel.: +33 4 42 19 92 63; fax: +33 4 42 19 91 65.
E-mail address: olivia.coindreau@irsn.fr (O. Coindreau).

0022-3115/$ - see front matter © 2010 Elsevier B.V. All rights reserved.
doi:10.1016/j.jnucmat.2010.07.038

Table 1
Gibbs energy (in kJ/mol) of formation of zirconia and zirconium nitride at 627, 827, 1027, 1227 °C.

Material	Temperature			
	627 °C	827 °C	1027 °C	1227 °C
ZrO_2	−929	−892	−855	−818
ZrN	−280	−262	−243	−225

Considering the Gibbs energy of formation of ZrO_2 and ZrN (given in Table 1), it can be concluded that ZrO_2 formation is energetically more favorable than ZrN formation as long as oxygen consumption is not nearly complete. Based on the Gibbs energy given in Table 1, and without any consideration of reaction kinetics, it can be computed that, for a total pressure of one bar, nitriding theoretically takes place at the detriment of ZrO_2 formation if oxygen partial pressure is smaller than 2.1×10^{-38} bar at 627 °C or smaller than 2.2×10^{-21} bar at 1227 °C. Actually, experimental investigations show that nitriding of zirconia can be achieved directly in a nitrogen atmosphere only at temperature above 1400 °C [6,7] and in the presence of an oxygen getter. For lower temperatures, Gilles's experiments have demonstrated that it is possible to nitridate zirconia by a reaction of ZrO_2/ZrN mixtures in NH_3 [8,9].

It must be underlined that, in addition to the dioxide (ZrO_2) and nitride (ZrN) phases mentioned above, zirconium with dissolved oxygen (α-Zr(O)), zirconium with dissolved nitrogen (α-Zr(N)) as well as oxynitride phases ($ZrO_{2-2x}N_{4x/3}$), brought to light by investigations in the Zr–O–N system [8,6], can be encountered.

Their formation can be described by the following equation:

$$ZrO_2 + \frac{2x}{3}N_2 \rightarrow ZrO_{2-2x}N_{4x/3} + xO_2 \quad (3)$$

Unfortunately, few thermodynamic data on the oxynitride phases formation exist in the literature.

In spite that the oxidation reaction is thermodynamically much more favorable than the nitriding one, nitride formation has been observed when Zircaloy is oxidized in O_2–N_2 gas mixtures at high temperature [10]. Moreover, it was experimented for a long time that oxidation kinetics of Zircaloy in the 600–1000 °C temperature range is significantly higher in O_2–N_2 gas mixtures than in O_2 or H_2O [11,10]. This detrimental role of nitrogen is particularly important under starvation conditions which can occur either globally (i.e. if oxygen is absent or nearly absent from the atmosphere) or locally (i.e. if oxygen is absent, for instance, in the cracks formed in the oxide layer). As thermodynamic considerations have demonstrated, the oxygen concentration has to be extremely reduced for the nitride to be the stable product. However, nitriding can take place if the oxidation kinetics is lower than the nitriding kinetics and this can occur for partial pressure of oxygen far greater than the partial pressure at the thermodynamic equilibrium. Thus, it is of great importance to consider the kinetics of the individual reaction steps describing the oxidation mechanism to account for nitride formation during air oxidation. When Zircaloy-4 is scaled in air, two different kinetic regimes succeed, separated by a kinetic transition named breakaway. The oxide microstructure as well as the oxidation mechanism are radically different before and after the kinetic transition. Also is the extent of nitriding which is much more important in the post-transition regime.

A summary of kinetic data and postulated oxidation mechanisms is proposed in Section 2 with an emphasize on the experimental data obtained at IRSN in the framework of the MOZART program [12] since these data are used to derive our model. Finally, a comparison between the measured and the simulated weight gain of Zircaloy-4 cladding samples oxidized in air is carried out in Section 4.

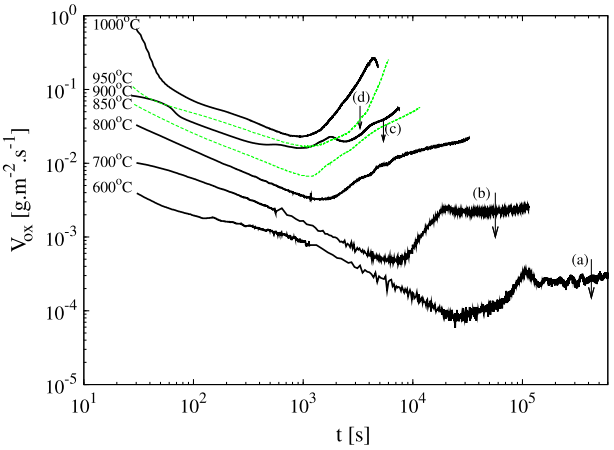

Fig. 1. Scaling rate for air oxidation of Zircaloy-4 between 600 and 1000 °C. Samples are short open segments cut from Pressurized Water Reactor cladding tubes of 20 mm length (600, 700, 800 and 850 °C) or 7 mm length (900, 950 and 1000 °C). The air flow rate is 500 mL min^{-1} except for the experiment at 1000 °C for which 1000 mL min^{-1} is used (more details are given in [12]). Arrows indicate the duration of oxidation reached for samples shown in Fig. 3.

2. Separate-effect tests analysis

A number of studies have been carried out to investigate the oxidation behavior of zirconium and its alloys in air. The considerable influence of nitrogen when zirconium is scaled in air was pointed out a long time ago [13,11] and a number of kinetics measurements were carried out [14,15], some of them in oxygen–nitrogen atmospheres of different compositions [16]. More recently, the results of experimental programs aiming at obtaining new kinetic data and at improving our understanding of the air oxidation process were reported [10,12,17].

It was shown in [12] that in the 600–1000 °C temperature range, the oxidation kinetics obeys initially a parabolic or quasi-parabolic relationship transforming to a faster relationship after the advent of the kinetic transition, associated with the cracking of the oxide and the transformation of the dense oxide layer into a porous, cracked oxide scale. An illustration of the air oxidation kinetics behavior of Zircaloy-4 at temperatures of 600–1000 °C is given in Fig. 1. It must be emphasized that these thermogravimetric data were obtained with a high air flow rate to avoid global oxygen starvation. An analysis of these kinetic curves and the associated oxidation mechanisms is done hereafter.

2.1. Pre-transition regime

During the pre-transition period, the oxidation rate can be described by a parabolic or quasi-parabolic law. The parabolic behavior can be explained by the growth of a dense oxide scale and dissolution of oxygen in the underlying metal. It is the diffusion of oxygen vacancies in the oxide scale which controls the oxidation rate. During this period, the oxide scale is considered as protective since an increase of its thickness, by increasing the diffusion length, leads to a decrease of the oxidation rate. In this early stage, the influence of nitrogen is likely to be relatively weak. It was shown by Rosa and Smeltzer [16] that, at 850 °C, the parabolic rate increases with increasing nitrogen content in O_2/N_2 gas mixture. It was suggested that the oxide containing nitrogen has an increased concentration of oxygen vacancies and thus leads to an higher parabolic rate constant. Such an influence of nitrogen was not put in evidence in the experiments of Duriez et al. [12] where the parabolic rate constants derived from isothermal air oxidation tests are close to those measured in steam oxidation experiments [18].

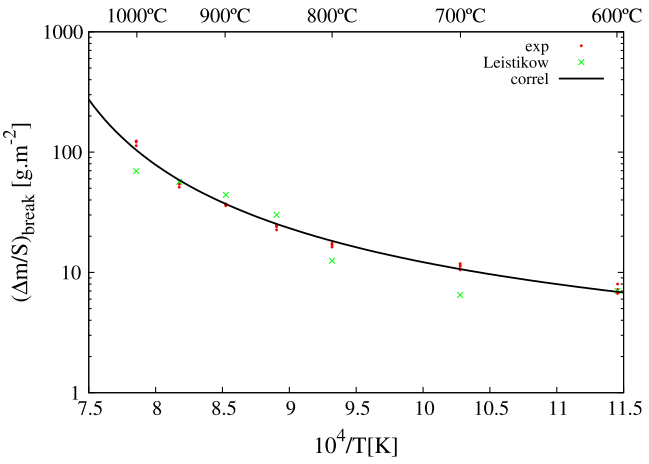

Fig. 2. Weight gains at transition measured under air in IRSN experiments ('exp'), under steam ('Leistikow', extracted from [18]) and predicted by Eq. (11) ('correl').

It must be underlined that the air flow rate used in [12] to oxidize samples was sufficiently high to prevent any oxygen starvation. The conclusion of [12] indicating that the protective zirconia scales grown in air and steam have similar properties regarding oxygen diffusion can be considered as valid only if there is a sufficient amount of oxygen in the gas mixture. Otherwise, it is likely that nitrogen interacts with the oxide scale, changing its diffusion properties and consequently the oxidation kinetics. However, it seems that below 1000 °C, the role of nitrogen in the pre-transition regime is relatively weak.

2.2. Kinetic transition

In the 600–1000 °C temperature range, it was shown that it exists a kinetic transition whatever the oxidant is (oxygen, steam or air). The position of the kinetic transition is determined by the minimum of the weight gain rate. In the experiments carried out by Duriez et al. [12] and reported in Fig. 1, the kinetic transition occurs after 410 min at 600 °C and after 14 min at 1000 °C. The corresponding weight gains are higher with increasing temperatures and are quite similar to those measured in steam oxidation [18] (see Fig. 2). In air atmospheres and in the temperature range investigated, the transition is associated to the formation of radial cracks penetrating close to the metal/oxide interface. The origin of crack formation can be attributed to several possible mechanisms among which the oxide transformation from the tetragonal to the monoclinic form [14,19] (more details are given afterwards). This mechanism results in the formation of cracks in the outer layer of the oxide, transforming the dense oxide layer into a porous, cracked oxide layer. This microstructural change damages the corrosion resistance by decreasing the diffusion path of oxygen and nitrogen in the zirconia layer. After the kinetic transition, the oxidation curve is not parabolic indicating that the oxidation rate is no more controlled by the diffusion of oxygen through the oxide layer.

2.3. Post-transition regime

After the transition, the kinetics behavior exhibits differences between the low temperature range (600–700 °C) and the high temperature range (800–1000 °C).

For the low temperature range, we can observe in Fig. 1 that after having reached its minimum value, the oxidation rate increases and then remains nearly constant. It was also observed on the corresponding metallographies that the cracking responsible for the kinetic transition occurs approximately at the same time on the whole sample. We can assume that the relatively short increasing portion of the oxidation curve corresponds to the time needed for cracking to propagate to the whole surface sample. When the oxidation rate stabilizes, corresponding to a linear oxidation kinetics, it is likely that the whole sample experiences the same post-transition kinetics. This is supported by Fig. 3a and b showing that the whole sample has the same aspect when the oxidation has reached a constant value. The various articles dedicated to the oxidation of Zircaloy-4 under steam or oxygen at the temperature of 500 °C also reported that post-transition oxidation curves are linear. Different explanations were proposed (a succession of quasi-parabolic periods, a rate-limiting step of diffusion in a dense layer of constant thickness close to the metal/oxide interface) but they were discarded by gravimetry experiments carried out at 500 and 550 °C on Zircaloy-4 samples [20]. It seems that no rate-limiting step can be assumed for steam oxidation in the post-transition regime and the authors suggest that the diffusing species in the porous outer layer (surface hydroxyl groups $OH_O^{\cdot}$) are different from those in the dense layer (oxygen ions O_O^x). The conclusions are quite different with the ZrNbO alloy [21]. The assumption of a rate-limiting step can be made in the post-transition stage with an interface step as the probable rate-controlling step but neither the location (i.e. at the external interface, at the porous/dense layer interface or at the metal/oxide interface) nor the rate-limiting step was put in evidence. It must be underlined that despite differences in the oxidant species (oxygen and hydrogen in steam, oxygen and nitrogen in air), the post-transition oxidation rate under steam and under air are relatively close (see Table 2). The role of nitrogen can consequently be considered as weak in the 600–800 °C temperature range and as long as oxygen starvation is prevented. However, to determine the influence of partial pressures in oxygen and nitrogen on the oxidation rate, the oxidation mechanism should be clarified and the rate-limiting step identified.

In the high temperature range, the oxidation behavior is quite different with the oxidation rate that does not stop increasing until the experiment is stopped. Actually, the oxidation decreases when the experiment lasts for a sufficiently long time for the equivalent cladding reacted (ECR) to be very high. For these samples, cracking does not occur everywhere simultaneously on the surface (see Fig. 3c and d). At around 15% ECR, it appears that some parts of the sample are still in the pre-transition state whereas the others exhibit a microstructure typical of the post-transition regime. Metallographies of Zircaloy-4 samples oxidized in air at 850 °C and above show that the post-transition oxide is cracked, porous and nitrided. Zirconium nitride particles can be seen close to the metal/oxide interface and it is thought that the high oxidation rates in the post-transition regime are due to simultaneous oxidation and nitriding reactions [11,12]. Contrary to the pre-transition regime and to the post-transition regime at low temperature (i.e. below 800 °C), nitrogen seems to play a critical role in the post-transition regime at high temperature. Despite relatively high air flow rates, it is likely that oxygen starvation occurs in the cracks of the oxide. The oxygen partial pressure in the cracks is low enough for the oxidation kinetics to be lower than the nitriding one, enabling zirconium nitride or oxynitride formation. When the oxygen partial pressure increases in the cracks of the oxide, the oxidation kinetics becomes higher than the nitriding one and the nitride particles are re-oxidized (since the oxide is thermodynamically much more stable than the nitride). This reaction releases nitrogen in the oxide or in the metal and results in a volume increase since the molar volume of the oxide is greater than the molar volume of the nitride. This oxi-nitriding mechanism is responsible for the "micro-porous" aspect of the oxide and of the fast degradation of the cladding. It can consequently be thought that the increase of the scaling rate in the post-transition regime

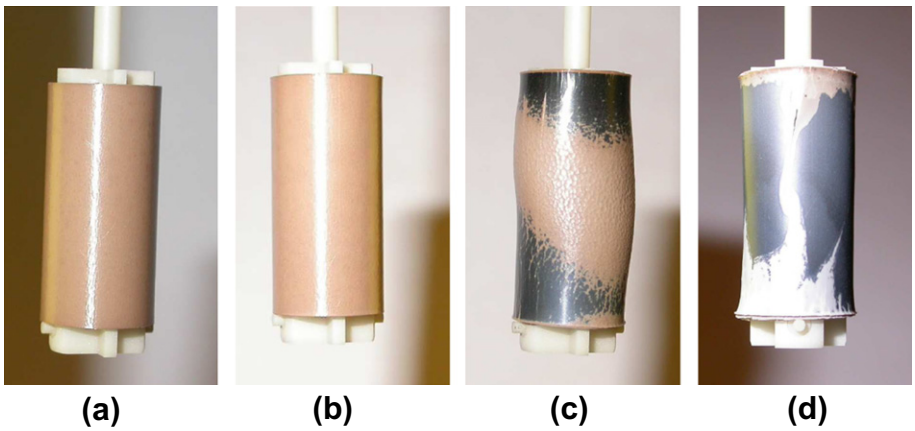

Fig. 3. Photographs of partially oxidized samples (around 15% equivalent cladding reacted) at 600 °C (a), 700 °C (b), 850 °C (c) and 950 °C (d). Times needed to reach this oxidation state are noted in Fig. 1.

Table 2
Post-transition oxidation rate (in $g\,m^{-2}\,s^{-1}$) as a function of the temperature (T) extracted from the literature and from the present study. The oxidant medium is either steam or air at atmospheric pressure.

T (°C)	Cox [22] steam	Denis [23] steam	Boase [15] air	Present study air
600	4.89×10^{-4}	3.59×10^{-4}	3.38×10^{-4}	3×10^{-4}
700	3.53×10^{-3}	2.84×10^{-3}	2.14×10^{-3}	2×10^{-3}

observed in IRSN experiments results from, at least, the following phenomena:

- A non-uniformity of the kinetic transition on the sample. As long as the kinetic transition has not occurred on the whole sample, the global kinetics results from the average between the pre-transition kinetics and the post-transition kinetics. As demonstrated in Section 3.4, the subsequent kinetics is accelerated.
- An important creep of the sample resulting in an increased surface exposed to the air atmosphere. Evans has early suggested that strong sample deformation generally observed in air oxidation experiments can be a consequence of the nitriding-oxidation sequence [11]. Indeed, it was observed in IRSN experiments that sample deformation is strong only where nitriding has occurred. Such deformation is likely to be due to creep of the metal upon the stresses applied by the oxide scale when nitride particles convert into oxide. It induces a very significant increase of the surface exposed to air, which undoubtedly contributes to the post-breakaway acceleration.

3. Code modeling

3.1. Oxidation modeling in the ASTEC code

ASTEC is a severe accident integral code jointly developed by IRSN (in France) and GRS (in Germany) [24]. This is a system of calculation codes that simulate the complete scenario of a hypothetical severe accident in a nuclear light water reactor. It is used by IRSN to perform safety analysis with a great number of scenarios to be studied. In this context, the development of modeling for ASTEC code application is a compromise between modeling detail and calculation time.

The ICARE module of ASTEC simulates the in-vessel core degradation and deals with, in particular, the oxidation of Zircaloy cladding. The amount of oxidation depends on one hand on the reaction kinetics and on the other hand on air availability at the cladding-fluid interface. The oxidation reaction kinetics is calculated first, indicating the oxygen mass flux requested by the oxidation reaction. The mass flux really available by oxygen diffusion within the fluid phase is then computed and the limiting step (oxidation reaction or oxygen diffusion within the fluid phase) identified. If starvation occurs (i.e. oxygen diffusion within the fluid phase is the limiting step) the weight gain depends on the oxygen mass flux at the cladding-fluid interface and is a function of the partial pressure of oxygen in the fluid. Otherwise, the weight gain is computed following the oxidation reaction kinetics. The energy released during the oxidation process results from ZrO_2 and α-Zr(O) formation.

Compared to steam oxidation, there is no steam molecules dissociation (which is an endothermic reaction) under air oxidizing conditions. The total energy involved in the air oxidation process is consequently greater than that in steam for a same number of moles of zirconium oxidized. The treatment of air oxidation kinetics by the ICARE module is based on mass correlations to evaluate the growth of zirconia and α-Zr(O) layers in non-starvation conditions. The previous model of ICARE described the air oxidation reaction kinetics by a parabolic law, with the parabolic rate constant recommended by Powers et al. [1]. It was found that this model fails in simulating the accelerated oxidation observed in experiments. Taking into account experimental observations and kinetic data obtained at IRSN and displayed in Fig. 4, a new model

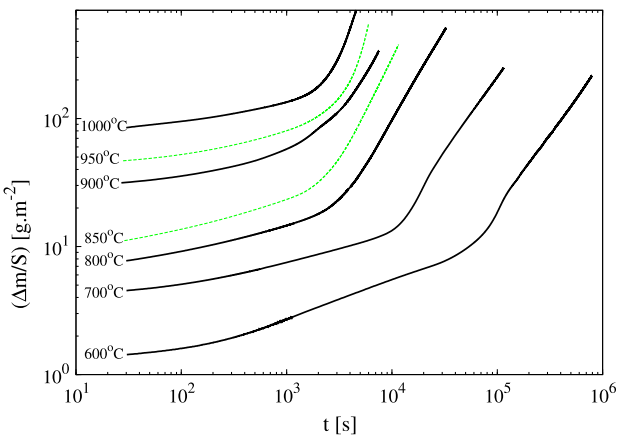

Fig. 4. Weight gain for air oxidation of Zircaloy-4 between 600 and 1000 °C.

for air oxidation was designed. The role of nitrogen in the air oxidation process is not explicitly accounted for but implicitly taken into account in the oxidation kinetics, as described hereafter.

3.2. Oxidation kinetics in the pre-transition regime

In the pre-transition regime, the total weight gain is described by a parabolic law:

$$\frac{d(\Delta m/S)^2}{dt} = K_p \tag{4}$$

with $\Delta m/S$ the weight gain per surface unit in kg m^{-2}, t the exposure time in seconds and K_p the parabolic rate constant in kg^2 m^{-4} s^{-1}. Assuming that K_p is a temperature dependent Arrhenius-type function, the following correlation, derived from the data presented in Fig. 4 is used:

$$K_p = A_{ma} exp\left(\frac{-B_{ma}}{RT}\right) \tag{5}$$

with $A_{ma} = 96.48$ kg^2 m^{-4} s^{-1}, $B_{ma} = -1.899 \times 10^5$ J mol^{-1}, T the temperature in K and R the perfect gas constant in J mol^{-1} K^{-1}.

It is thus implicitly assumed that oxygen diffusion through the zirconia layer is the limiting step.

3.3. Breakaway transition

The weight gain at which occurs the kinetic transition increases with increasing temperature. To derive a suitable correlation between this critical weight gain, noted $(\frac{\Delta m}{S})_{break}$, and the temperature, we have assumed that the breakaway transition is linked with the tetragonal to monoclinic zirconia transformation. This hypothesis of stress relaxation, associated to the tetragonal to monoclinic transformation, has been proposed for a long time [14,25] and was used to evaluate the characteristic thickness where the oxide breaks away in the temperature range 400–800 °C [26]. Despite that this hypothesis was recently discarded [27,28], it is used here as no satisfactory mechanism has been proposed ever since to explain the origin of the kinetic transition.

The oxide formed between 600 °C and 1150 °C is expected to be monoclinic zirconia (noted m-ZrO_2). But tetragonal zirconia (noted t-ZrO_2) can also be found, being stabilized at subcritical temperatures by fine grain size, hydrostatic pressure, or a very high defect concentration [29]. The presence of tetragonal zirconia in the oxide scale is generally attributed to high compressive stresses [30]. The free energy change of t-ZrO_2 to m-ZrO_2, $\Delta G(\mathrm{t} \rightarrow \mathrm{m})$, can be written as:

$$\Delta G(\mathrm{t} \rightarrow \mathrm{m}) = G^0_{\mathrm{m}}(T) - G^0_{\mathrm{t}}(T) + (u_{\mathrm{m}} - u_{\mathrm{t}}) \tag{6}$$

with $G^0_{\mathrm{m}}(T)$ (resp. $G^0_{\mathrm{t}}(T)$) the standard free energy of m-ZrO_2 (resp. t-ZrO_2) formation in J mol^{-1} and u_{m} (resp. u_{t}) the compressive strain–energy of m-ZrO_2 (resp. t-ZrO_2) in J mol^{-1}.

The monoclinic zirconia is thermodynamically stable at temperatures below 1174 °C and the enthalpy of transformation of t-ZrO_2 to m-ZrO_2 is $H_{tr} = -5.94 \times 10^3$ J mol^{-1} [31]. Assuming that the heat capacities of the two polymorphs are independent of temperature, the free energy difference between m-ZrO_2 and t-ZrO_2 can be approximated by:

$$G^0_{\mathrm{m}}(T) - G^0_{\mathrm{t}}(T) = H_{tr}\left(1 - \frac{T}{T_b}\right) \quad \text{where } T_b = 1174\ ^\circ\mathrm{C} \tag{7}$$

The tetragonal phase can be found below T_b if $\Delta G(\mathrm{t} \rightarrow \mathrm{m})$ is positive i.e. if:

$$(u_{\mathrm{m}} - u_{\mathrm{t}}) > -\left[G^0_{\mathrm{m}}(T) - G^0_{\mathrm{t}}(T)\right] \tag{8}$$

It can be assumed that the compressive strain–energy is greater for the monoclinic phase (having a greater Pilling–Bedworth ratio). In addition, it was shown by Raman spectroscopy [32] that compressive stresses in the oxide layer are larger at the metal–oxide interface and reduce away from this interface. It can thus be conjectured that the compressive strain–energy difference is maximum near the Zr/ZrO_2 interface (where compressive stresses are maximum) and decrease away from the interface (due to the decrease of compressive stresses). As the oxide grows, the compressive strain–energy difference at the oxide–gas interface decreases. When the oxide reaches a critical thickness, the compressive strain–energy difference is not high enough to keep the tetragonal phase stable. The thermodynamically stable m-ZrO_2 tends to form upon the surface of t-ZrO_2. Due to its larger volume, the m-ZrO_2 stresses the underlying t-ZrO_2 causing extensive crack formation and propagation. The breakaway can thus be thought to be related to the tetragonal–monoclinic transformation of ZrO_2 accompanied by crack formation.

It is assumed that the strain–energy difference can be written as:

$$u_{\mathrm{m}} - u_{\mathrm{t}} = f\left(\frac{1}{(\Delta m/S)}\right) = \frac{A}{(\Delta m/S)^B} \tag{9}$$

Thus, the critical mass gain $(\Delta m/S)_{break}$ corresponds to:

$$\frac{A}{(\Delta m/S)^B_{break}} = -\left[G^0_{\mathrm{m}}(T) - G^0_{\mathrm{t}}(T)\right] = -H_{tr}\left(1 - \frac{T}{T_b}\right) \tag{10}$$

Experimental weight gains at transition were used to determine the A and B coefficients in Eq. (10) and the following correlation was obtained:

$$\left(\frac{\Delta m}{S}\right)_{break} = 3.1910^5 \left(\frac{T_b}{H_{tr}(T - T_b)}\right)^{2.27} \tag{11}$$

Fig. 2 shows that this correlation is well adapted. The correlation predicts that the critical mass gain goes to infinite when the temperature tends to T_b, indicating that breakaway becomes impossible when temperature reaches T_b. Such a behavior has indeed been verified experimentally in air [11,12], and also in steam [18]. The $(\frac{\Delta m}{S})_{break}$ criterion given by Eq. (11) is used in the ICARE module to model the kinetic transition in the 600–1000 °C temperature range.

3.4. Oxidation kinetics in the post-transition regime

After the kinetic transition, it was shown in the previous section that the oxidation rate increases. This accelerated oxidation behavior can be attributed to the progressive propagation of the kinetic transition to the whole sample. For the low temperature range, the oxidation rate quickly stabilizes with a sample exhibiting a uniform surface. For the high temperature range, such a steady state is not achieved at the end of the experiment but it is likely that a steady state could also be reached in other conditions (more important cladding thickness for instance). Assuming that the post-transition kinetics is linear, it can be shown that the oxidation rate increases as long as the breakaway propagates. In [33], the post-breakaway kinetic curves have been satisfactorily simulated by modeling the frequency of appearance of sections in the post-transition regime by a parabolic law:

$$\gamma = \gamma_0 (t - t_0)^2 \tag{12}$$

where γ is the frequency of post-transition sections appearance (in number m^{-2} s^{-1}), t the time in seconds and t_0 the time at breakaway initiation.

The fraction of the sample surface still in the pre-transition regime consequently evolves as:

$$f_{pre-tr} = exp\left(\frac{-s_0 \gamma_0 (t - t_0)^3}{3}\right) \tag{13}$$

The oxidation rate variation with time, resulting from the progressive transition from parabolic to linear law, is:

$$V_{ox} = exp\left(\frac{-s_0\gamma_0(t-t_0)^3}{3}\right)\frac{\sqrt{K_p}}{2\sqrt{t}} + \left(1 - exp\left(\frac{-s_0\gamma_0(t-t_0)^3}{3}\right)\right)K_l \quad (14)$$

A simpler modeling was adopted in ICARE and its validity, compared to the above-mentioned approach, is performed afterwards. During breakaway propagation, corresponding to an oxidation rate increase, the kinetics is modeled in ICARE by an accelerated law:

$$\frac{d(\Delta m/S)^{0.5}}{dt} = K_a \quad (15)$$

with K_a the accelerated rate constant in $kg^{0.5}\,m^{-1}\,s^{-1}$. For Zircaloy-4, a suitable correlation for K_a is $K_a = A_{ma}\,exp(\frac{-B_{ma}}{RT})$ with $A_{ma} = 0.745\ kg^{0.5}\,m^{-1}\,s^{-1}$, $B_{ma} = -9.5 \times 10^4\ J\,mol^{-1}$, T the temperature in K and R the perfect gas constant in $J\,mol^{-1}\,K^{-1}$.

Up to 800 °C, it was shown that the oxidation rate, after increasing, remains nearly constant. Moreover, oxidation rates derived from the correlations found in the literature are relatively close to each other (see Table 2). When oxidation rate predicted by Eq. (15) exceeds the oxidation rate given by the correlation of Boase et al. [15], the kinetics is modeled by the following linear law:

$$\frac{d(\Delta m/S)}{dt} = V_{ox} = K_l \quad (16)$$

with K_l the linear rate constant in $kg\,m^{-2}\,s^{-1}$, evolving with the temperature according to the correlation of Boase et al. [15].

Above 800 °C, and for the sample geometry examined here, the oxidation rate does not stop increasing. It is consequently modeled by the accelerated law up to the complete oxidation, implicitly assuming that no steady state is achieved.

In the modeling adopted in ICARE for breakaway propagation, the oxidation rate increases linearly with time (derived from Eq. (15), $V_{ox} = 2K_a^2 t$). This approach was compared to the modeling of the frequency of appearance of post-breakaway sections by a parabolic law. As illustrated in Fig. 5, the oxidation rate derived from Eq. (15) compares well with the result of Eq. (14) at 700°C. This justifies the modeling of the progressive transition from a parabolic to a linear law by an accelerated law in ICARE.

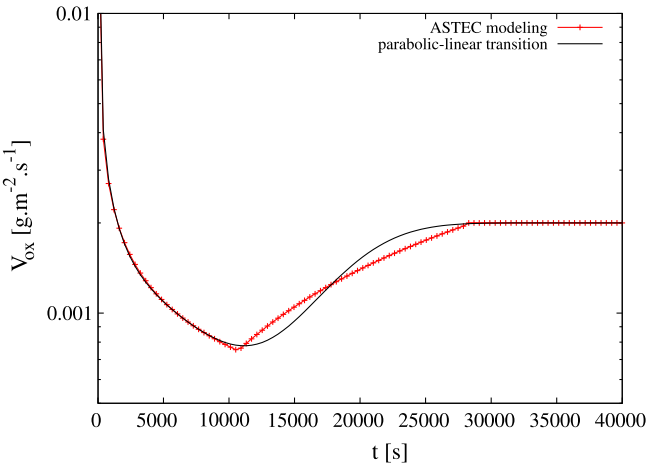

Fig. 5. Comparison of the oxidation rate at 700 °C using Eq. (14) ('parabolic-linear transition') and Eq. (15) ('ASTEC modeling'). The value for $s_0\gamma_0$ is set to $5 \times 10^{-13}\ s^{-3}$.

4. ICARE/CATHARE V2 calculations

To evaluate the modeling described above, isothermal and non-isothermal oxidation thermogravimetric results obtained at IRSN [12] and FZK [10] with different air flow conditions have been simulated.

4.1. Nodalization and physical model options

The experimental set-ups have been modeled using the degradation module of ASTEC named ICARE coupled with the thermal-hydraulics system code CATHARE [34]. The modeling is mono-dimensional, with 10 axial meshes and one fluid channel. Double face oxidation is calculated for the cylindrical Zircaloy sample. The heating phase of the experiment is not modeled. To simulate the isothermal phase, the furnace external wall temperature is set to the experimental temperature. Air is represented as a mixture consisting of O_2 (21% molar fraction) and N_2 (79% molar fraction). Temperature, mass flow rate, non-condensable mass fractions, and void fraction are imposed as inlet boundary conditions and a pressure outlet boundary condition is used. Heat exchanges by conduction, convection and radiation are modeled. The convective heat transfer coefficient h between the gas and the walls is computed from:

$$h = Nu\frac{\lambda_G}{D_H} \quad (17)$$

where Nu is the Nusselt number, λ_G is the gaseous conductivity, and D_H is the hydraulic diameter.

The Nusselt number is computed from specific correlations according to the flow regime, the fluid properties, the wall temperature, and the geometry. The computation of radiation heat transfer between the cladding, the furnace, and the gas is based on the net radiation enclosure model which consider surface to surface radiation and the interaction between radiation and the gas filling the enclosure. An anisotropic correction is made to take into account the convexity of surfaces such as fuel rods and shrouds. The reflection anisotropic factor is set to 0.15 for the furnace and to 0.5 for the cladding (for a totally isotropic surface, this factor is set to 0). The gas is assumed to be a grey gas i.e. absorption (and therefore emission) properties are wavelength independent. The view factor between the cladding and the furnace is automatically updated according to core degradation process.

4.2. Results

Simulations were performed at 600, 700, 800, 900, and 1000 °C. The air flow rate is 500 mL min^{-1} in IRSN experiments (except for the experiment at 1000 °C for which 1000 mL min^{-1} is used) and 167 mL min^{-1} in FZK experiments. Samples are short open segments cut from Pressurized Water Reactor cladding tubes of 20 mm length (IRSN experiments at 600, 700, 800 °C), 10 mm length (FZK experiments at 800, 1000 °C) or 7 mm length (IRSN experiments at 900, 1000 °C). In FZK experiments, samples were oxidized till approximately 16 wt% (at 800 °C) or 25 wt% (at 1000 °C) was reached (a complete oxidation leads to a mass gain of 35 wt%). All experiments take place at atmospheric pressure. Comparisons between experimental and numerical results are shown in Fig. 6. The simulations were performed with the model described in this paper and with the previous model which did not take into account the breakaway transition (the kinetics follows a parabolic law during the whole scaling experiment with the correlation for the parabolic rate recommended by Powers et al. [1]). The previous model largely overestimates the time for complete oxidation and the results are in poor agreement with

observations. By comparison, the actual model provides a much better agreement.

At low temperatures (600–700 °C), there is a good agreement between measured and computed mass gain. The breakaway transition at 600 °C (700 °C, respectively) is observed after about 414 min (90 min, respectively) in the experiments and 524 min (77 min, respectively) in the modeling. This means that the correlation taken for the parabolic rate constant (Eq. (5)) succeeds in reproducing the time at which the critical weight gain is reached. The slight difference observed between experimental and calculated time at transition can be due to:

– The modeling of the pre-breakaway kinetics by a parabolic law, whereas experiments have shown that the parabolic law is not strictly followed during the whole pre-breakaway regime.
– The model error in cladding temperature prediction. As the parabolic coefficient is strongly temperature dependent, the cladding temperature has to be as close as possible to experimental cladding temperature. The computed weight gain is not only sensitive to the air oxidation model but also to the thermal-hydraulic model.

The post-breakaway oxidation behavior is well reproduced with the correlation of Boase [15] for the linear rate constant.

At 800 °C, similar oxidation rates were measured in IRSN and FZK experiments, despite differences in sample size and air flow rate. This probably indicates that in both cases sufficiently high air flow rates were used to prevent starvation. If starvation occurred, the limiting-mechanism would be the oxygen flux to the cladding-fluid interface. The oxygen flux depends on the O_2 partial

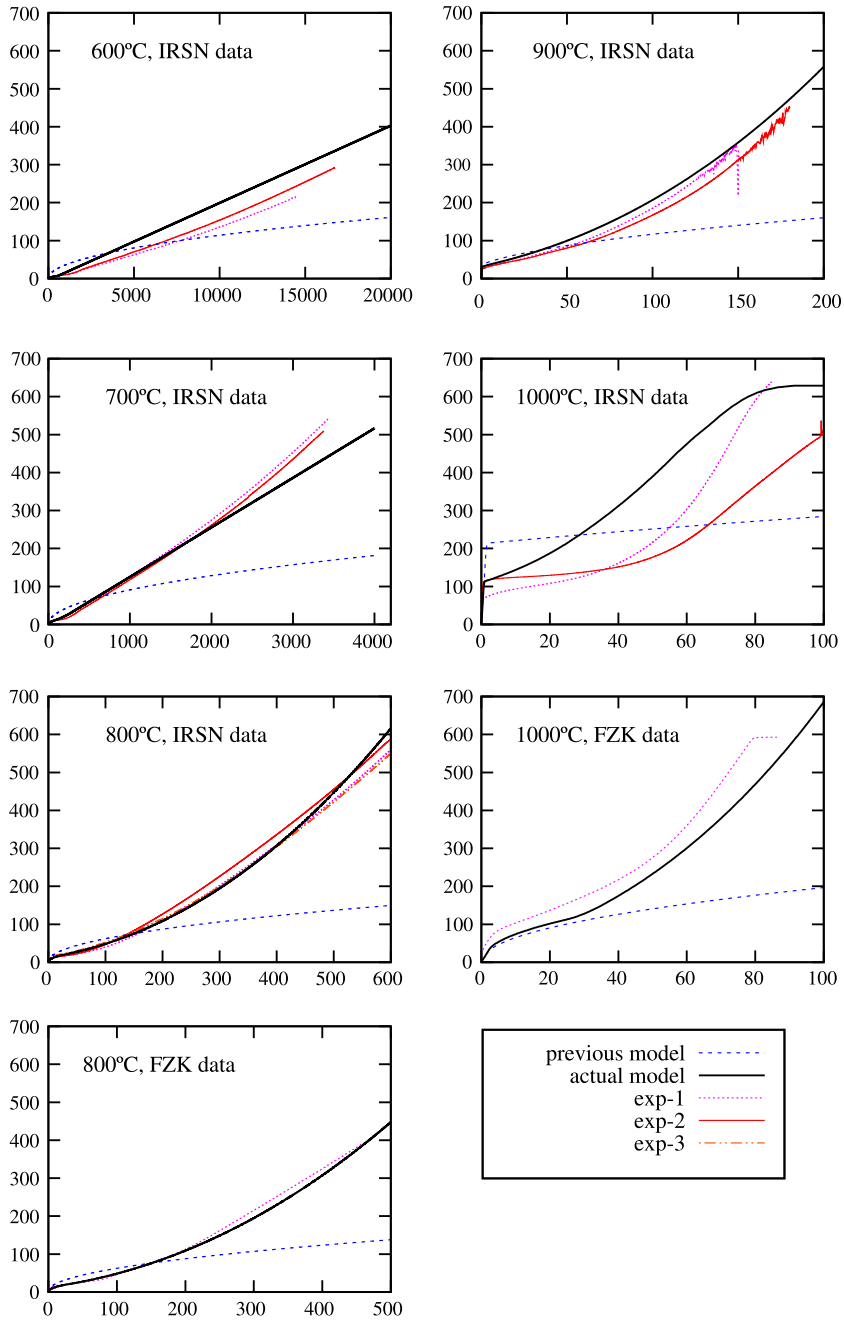

Fig. 6. Comparison between experimental and calculated weight gain (in g m^{-2}) versus time (in min). Experimental data are isothermal oxidation thermogravimetric results obtained at IRSN [12] or FZK [10].

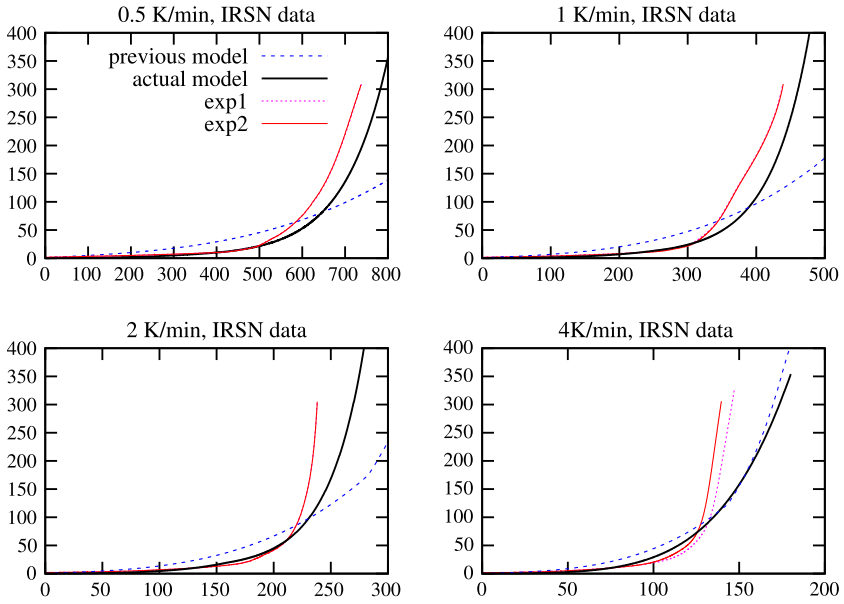

Fig. 7. Comparison between experimental and calculated weight gain (in g m^{-2}) versus time (in min) for non-isothermal oxidation thermogramimetric tests.

pressure in the fluid and is all the higher than the flow rate is important. Indeed, due to the oxygen uptake by the oxidation reaction, there is an axial profile of the oxygen partial pressure along the sample. In the conditions of IRSN and FZK experiments, similar oxidation rates were measured, independently from the air flow rate. Under these non-starvation conditions, the numerical results are in close agreement with experimental data. The model is able to capture the pre-breakaway kinetics, the time needed to reach the kinetic transition and the post-breakaway kinetics. Satisfactory results are also obtained at 900 °C.

At 1000 °C, the results of experiments carried out at IRSN and FZK significantly differ. Under high air flow conditions (IRSN experiments), the oxidation rate is at first very high, then remains nearly constant and finally increases again. By comparison, low air flow rates (FZK experiments) lead to less important mass gain at the very beginning. For this rather high temperature, the oxidation is very fast. If the air flow rate is not sufficiently high, this can lead to the complete O_2 consumption, at least for a short time at the transient beginning. Under these conditions, the availability of oxygen is the limiting step. This explains why oxidation rates are weaker in FZK experiments, carried out with lower air flow rates. The model is able to capture the differences in kinetics at the beginning of the oxidation process induced by different air flow conditions. The prediction of the kinetic transition is less accurate for high air flow conditions (one should also note that experiment results seem to be not well reproducible with noticeable differences between the two IRSN experimental curves). Under high air flow conditions, the oxidation kinetics is very fast at the transient beginning and the oxide layer rapidly reaches an important thickness. This leads to a sharp decrease of the oxidation rate (about 10 min after the beginning) since diffusion of the oxygen through the dense oxide layer is the limiting step in the pre-transition regime. In IRSN experiments, it takes about 30 min for the mass gain to reach the critical breakaway mass gain. In the calculation, the critical mass gain is reached very quickly. The underestimation of time needed to reach the kinetic transition could be due to the underestimation of the critical weight gain at this temperature, with respect to the experimental value (see Fig. 2). But part of the difficulty arises from the sharp increase in temperature at the air injection. The growth of the oxide layer is very quick and the kinetic transition, based on a critical weight gain, difficult to estimate. Indeed, a slight error made on the prediction on the weight gain can lead to an important error on the prediction of time needed to reach the kinetic transition. Under low air flow conditions, a better agreement is obtained. For the same reason as given previously, the predicted critical weight gain is underestimated, but this has a minor impact. In the pre-transition regime, the oxidation rate does not decrease as much as under high air flow conditions, being the oxide layer thinner. A slight error on critical weight gain prediction leads to a slight error on predicted time needed to reach the kinetic transition and the overall agreement is much better.

The validity of the model has also been evaluated by comparing measured and computed mass gain of Zircaloy-4 samples oxidized in non-isothermal conditions. Experimental data were acquired at IRSN by thermogravimetric analysis, in non-isothermal conditions with an heating rate ranging from 0.5 to 4 K min^{-1}. The air flow rate is 500 mL min^{-1} with 20 mm length samples. Under slow transient-heating conditions (up to 2 K min^{-1}), there is a rather good agreement between model predictions and experimental data (see Fig. 7). Compared to the predictions of the previous model, which did not take into account breakaway transition and accelerated kinetics, results are significantly improved. However, if the heating rate exceeds 4 K min^{-1}, the present model fails in capturing the acceleration of the oxidation kinetics. The detection of the kinetic transition is based on a critical weight gain which increases with increasing temperature. Under fast transient-heating conditions, the critical mass gain predicted by Eq. (11) quickly increases. At the same time, the weight gain of the sample, that follows a parabolic law in the pre-transition regime, does not increase as much. The mass gain consequently does not reach the critical mass gain necessary for the kinetic transition to occur. The simulated kinetics remains parabolic and the accelerated oxidation is only due to the increase of the parabolic rate constant as temperature rises.

5. Conclusions

The treatment of air oxidation in the ASTEC code is based on oxygen availability at the cladding-fluid interface. Under starvation conditions, oxygen diffusion within the fluid phase is the limiting step and the amount of oxidation depends on the oxygen partial pressure in the fluid. Under non-starvation conditions, a simple and semi-empirical model has been developed to simulate the Zir-

caloy-4 oxidation reaction kinetics. The model considers that the interaction between Zr and O_2 occurs, in a first stage, following a parabolic kinetics. Transition to post-breakaway oxidation is based on a critical value of the O_2 mass gain, function of the temperature. The correlation between the critical weight gain and the temperature is based on the assumption that breakaway transition is linked with the tetragonal to monoclinic zirconia transformation. At low temperature ($\leqslant$800 °C), the post-breakaway kinetics is modeled by an accelerated law (oxidation rate increases linearly with time) and then by a linear law. The accelerated law accounts for the progressive propagation of the kinetic transition, being the post-transition growth law linear. At high temperature (>800 °C), the air oxidation kinetics of the cladding sample material is modeled by an accelerated law. Actually, substantial degradation occurs before the progressive transition from parabolic to linear law is completed.

The air-oxidation model in the ASTEC code has first been assessed on isothermal oxidation thermogravimetric results coming from IRSN and FZK, for the temperature range between 600 and 1000 °C. Predictions of time needed to reach complete oxidation by using the parabolic rate law (previous model) are substantially higher than the experimental values. By comparison, the model described in this paper shows a much better agreement. The model improves the oxidation rate predictions in the temperature range investigated (600–1000 °C) and for different air flow conditions. Under non-isothermal conditions, the comparison of numerical simulations with experimental data have shown that the model is still valid if the heating rate does not exceed 2 K min^{-1}.

To build a more accurate model which directly simulates the oxi-nitriding mechanism responsible for the formation of porous oxide and fast clad degradation, a further theoretical and experimental work is required. Especially, the limiting-mechanism of reaction kinetics must be identified to quantify the effect of O_2 and N_2 partial pressure on oxidation and nitriding. Such a model will also improve the prediction of the reaction heat that at present is only due to the formation of ZrO_2 and then, for a given total mass gain, is probably overestimated. The assessment of the model against more integral tests will be also a key point to demonstrate that ASTEC code can be used, with sufficient assurance, for the simulation of reactor and spent fuel pool accidents scenarios, where Zircaloy cladding could be exposed to air or air–steam atmosphere.

Acknowledgments

Gaëtan Guillard from IRSN is thanked for its contribution to implement the model in the ASTEC code. Many thanks to Karim Keshk for its contribution during its end of studies training at IRSN. Dr Martin Steinbrück from FZK is also gratefully thanked for fruitful discussions.

References

[1] D.A. Powers, L.N. Kmetyk, R.C. Schmidt, A Review of the Technical Issues of Air Ingression During Severe Reactor Accidents, Tech. Rep. NUREG CR-6218, Sandia National Laboratories, 1994.
[2] V.L. Sailor, K.R. Perkins, J.R. Weeks, H.R. Connell, Severe Accident in Spent Fuel Pools in Support of Generic Safety, Tech. Rep. NUREG CR-4982, Broohaven National Laboratory, 1987.
[3] K. Natesan, W.K. Soppet, S. Basu, Low temperature air oxidation experiments at ANL, in: Proceedings of the CSARP Meeting, Crystal City, 2004.
[4] F.C. Iglesias, C.E.L. Hunt, F. Garisto, D.S. Cox, N.A. Keller, R.D. Barrand, J.R. Mitchell, R.F. O'Connor, Measured release kinetics of ruthenium from uranium oxides in air, in: Proceedings of the International Seminar on Fission Product Transport Processes during Reactor Accidents, Hemisphere Publishing Corp., Washington, DC, USA, 1990.
[5] P. Giordano, A. Auvinen, G. Brillant, J. Colombani, N. Davidovich, R. Dickson, T. Haste, T. Kärkelä, J.S. Lamy, C. Mun, D. Ohai, Y. Pontillon, M. Steinbrück, N. Vér, Progress in Nuclear Energy 52 (2010) 109–119.
[6] Y.B. Cheng, D.P. Thompson, Special Ceramics 9 (1992) 149–162.
[7] Y.B. Cheng, D.P. Thompson, Journal of American Ceramic Society 76 (3) (1993) 683–688.
[8] J.C. Gilles, Bulletin de la Societe Chimique de France 22 (1962) 2118–2122.
[9] R. Collongues, J.C. Gilles, A.M. Lejus, M. Perez y Jorba, D. Michel, Material Research Bulletin 2 (1967) 837–848.
[10] M. Steinbrück, Journal of Nuclear Materials 392 (2009) 531–544.
[11] E.B. Evans, N. Tsangarakis, H.B. Probst, N.J. Garibotti, Critical role of nitrogen during high temperature scaling of zirconium, in: Proceedings of the Conference on Metallurgical Society of AIME, 1972, pp. 248–282.
[12] C. Duriez, T. Dupont, B. Schmets, F. Enoch, Journal of Nuclear Materials 380 (2008) 30–45.
[13] C.J. Rosa, Journal of the Less-common Metals 16 (1968) 173–201.
[14] B. Cox, Oxidation of Zirconium and Its Alloys, vol. 5, 1976, pp. 173–391.
[15] D.G. Boase, T.T. Vandergraaf, Nuclear Technology 32 (1977) 60–70.
[16] C.J. Rosa, W.W. Smeltzer, Zeitschrift Fur Metallkunde 71 (1980) 470–475.
[17] C. Duriez, M. Steinbrück, D. Ohai, T. Meleg, J. Birchley, T. Haste, Nuclear Engineering and Design 239 (2009) 244–253.
[18] S. Leistikow, G. Schanz, H. Berg, A. Aly, Comprehensive presentation of extended Zircaloy-4 steam oxidation results 600–1600 °C, in: OECD-NEA-CSNI/IAEA Specialists' Meeting on Water Reactor Fuel Safety and Fission Product Release in Off-Normal and Accident Conditions, Denmark, 1983.
[19] W. Qin, C. Nam, H. Li, J.A. Szpunar, Acta Materialia 55 (2007) 1695–1701.
[20] M. Tupin, M. Pijolat, F. Valdivieso, M. Soustelle, A. Frichet, P. Barberis, Journal of Nuclear Materials 317 (2003) 130–144.
[21] M. Tupin, M. Pijolat, F. Valdivieso, M. Soustelle, Journal of Nuclear Materials 342 (2005) 108–118.
[22] B. Cox, A Method for Calculating the Transient Oxidation of Zircaloy, Tech. Rep. AECL 6784, Atomic Energy of Canada Limited, 1980.
[23] A. Denis, E. Moyano, E.A. Garcia, Journal of Nuclear Materials 110 (1982) 11–19.
[24] J.P. Van Dorsselaere, C. Seropian, P. Chatelard, F. Jacq, J. Fleurot, P. Giordano, N. Reinke, B. Schwinges, H.J. Allelein, W. Luther, Nuclear Technology 165 (2009) 293–307.
[25] G. Schanz, S. Leistikow, Microstructural reasons for mechanical oxide degradation (breakaway effects) and resulting kinetic anomalies of Zircaloy-4/steam-HT-oxidation, in: Proceedings of 8th International Congress on Metallic Corrosion, Mainz, Germany, vol. 2, 1981, pp. 1712–1717.
[26] H.I. Yoo, B.J. Koo, J.O. Hong, I.S. Hwang, Y.H. Jeong, Journal of Nuclear Materials 299 (2001) 235–241.
[27] P. Barberis, Journal of Nuclear Materials 226 (1995) 34–43.
[28] N. Pétigny, P. Barberis, C. Lemaignan, C. Valot, M. Lallemant, Journal of Nuclear Materials 280 (2000) 318–330.
[29] D. Douglas, International Atomic Energy Agency supplement 1971 (1971) 389–439.
[30] J. Godlewski, ASTM-STP 1245 (1994) 663–686.
[31] S. Xie, E. Iglesia, A.T. Bell, Chemistry of Materials 12 (2000) 2442–2447.
[32] J. Godlewski, P. Bouvier, G. Lucazeau, L. Fayette, ASTM-STP 1354 (1998) 877–900.
[33] M. Tupin, Approfondissement des mécanismes d'oxydation de deux alliages de zirconium: Zircaloy-4 et ZrNbO, sous oxygène et sous vapeur d'eau. comparaison des régimes cinétiquement limitants, Doctoral thesis, Ecole Nationale Supérieure des Mines de St-Etienne, 2002.
[34] P. Chatelard, J. Fleurot, O. Marchand, P. Drai, Assessment of the ICARE/CATHARE V1 severe accident code, in: Proceedings of ICONE 14, 14th International Conference on Nuclear Engineering, ASME, Miami (USA), 2006.